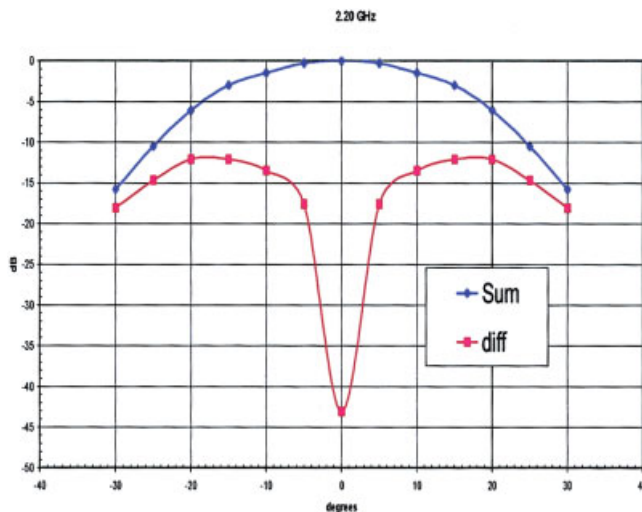**Figure 8** Phase distribution in the cross section of the mode couple for sum (left) and difference (right) patterns. [Color figure can be viewed in the online issue, which is available at www.interscience.wiley.com]

propagates, and the OMT for the data channel receives both the horizontal and vertical polarizations. We model the coupler (Fig. 3) by using the FDTD for only one pair of these rectangular guides. The size of the holes is optimized, based on several FDTD runs, in order to achieve proper coupling.

NUMERICAL AND MEASUREMENT RESULTS

The simulation results obtained by using the Body of Revolution FDTD code for the corrugated horn are shown in Figures 6 and 7.

Figure 9 Measured sum and difference patterns of the monopulse feed at 2.20 GHz. [Color figure can be viewed in the online issue, which is available at www.interscience.wiley.com]

The symmetric pattern with 10-dB taper in 20 degree is achieved for the E-, H- and 45-deg planes.

The phase distribution inside the mode coupler is shown for both the TE_{11} and TE_{21} modes in Figure 8. The coupling through the holes in the rectangular guides is evident from the figure. It is also evident that two modes generate different radiation patterns. In the TE_{21} mode (the right side), the opposite phase led to the field cancellation in the boresight and hence a sharp null.

The measurement results for both sum and difference patterns of the monopulse feed are shown in Figure 9. The 40-dB difference in the sum and difference channels in the boresight assures the high sensitivity of the target tracking.

REFERENCES

1. K.S. Yee, Numerical solution of initial boundary value problems involving Maxwell's equations in isotropic media, IEEE Trans Antennas Propagat AP-14 (1966), 302–307.
2. W. Yu and R. Mittra, CFDTD: Conformal finite-difference time-domain Maxwell's equations solver software and user's guide, Artech House, Boston, 2004.
3. A. Taflove and S.C. Hagness, Computational Electromangeics: The finite-difference time-domain method, 2nd ed., Artech House, Boston, 2000.
4. Y. Chen, R. Mittra, and P. Harms, Finite-difference time-domain algorithm for solving Maxwell's equations in rotationally symmetric geometries, IEEE Trans Microwave Theory Tech 44 (1996), 832–839.
5. P.J.B. Clarricoats and A.D. Olver, Corrugated horns for microwave antennas, IEE Publishing, England 1984.

© 2005 Wiley Periodicals, Inc.

UWB MICROSTRIP FILTER DESIGN USING A TIME-DOMAIN TECHNIQUE

Ibrahim Tekin
Telecommunications, Sabanci University
34956 Tuzla
Istanbul, Turkey

ABSTRACT: *A time-domain technique is proposed for ultra-wideband (UWB) microstrip-filter design. The design technique uses the reflection coefficient (S_{11}) specified in the frequency domain. When the frequency response of the UWB filter is given, the response will be approximated by a series of UWB pulses in the time domain. The UWB pulses are Gaussian pulses of the same bandwidth with different time delays. The method tries to duplicate the reflection scenario in the time domain for very narrow Gaussian pulses (to obtain the impulse response of the system) when the pulses are passed through the filter, and obtains the value of the filter coefficients based on the number of UWB pulses, amplitudes, and delays of the pulses. © 2005 Wiley Periodicals, Inc.*

1. INTRODUCTION

Ultra-wideband (UWB) technology has found military applications such as ground penetrating radar (GPR), wall penetrating radar, secure communications, and precision positioning/tracking [1, 2]. Recently, there has also been a growing interest in commercial use of UWB technology such as in wireless personal area networks (WPAN) [3, 4]. This interest has been the result of

increasing demand for much higher data rates on the order of hundreds of megabits, since future wireless networks will require very large transmission bandwidths to reach these data rates. Currently, most wireless data technologies such as Bluetooth and IEEE 802.11b have baseband signals up to tens of megabits, and the baseband signal is sent using an RF carrier, which is basically a narrowband communication technique. With the FCC's recent allocation of the frequency range from 3.1 to 10.6 GHz to UWB communications, it has become evident that UWB systems will play a crucial role in future wireless communication systems. A system such as a microstrip-line filter is referred to be UWB if the system has a bandwidth-to-center-frequency ratio greater than 0.25, or a bandwidth larger than 500 MHz.

For narrowband circuit designs, conventional frequency-domain techniques will suffice. However, for UWB, these design techniques become difficult to use and also less accurate, since the assumptions made for narrow bandwidth is violated. Time-domain techniques are better suited for ultra-wide bandwidth design due to the duality between frequency and time domain. We can use frequency-domain design techniques as the bandwidth is small. Similarly, we can use time-domain design techniques more successfully if the time duration is narrow, which is the case in UWB systems. UWB systems can be easily specified in frequency domain, however, it is not that easy to use the frequency-domain characteristics and design the system accordingly. The circuit's behavior, such as reflections from multiple points, is much easier to observe and realize in the time domain, and equally hard to see in frequency domain for UWB systems. This paper proposes the design of such a system using a time-domain technique that employs characteristics specified in the frequency domain. Frequency-domain microwave-filter design techniques can be found in [5, 6], where many conventional design techniques are mentioned, including lumped-element filter design using LC elements. Genetic algorithms are applied in the frequency domain to design microwave filters in order to find the values of these lumped components in [7, 8]. Digital-filter theory techniques have also been used in [9] for a transversal microwave-filter design. In [10, 11], scattering parameters were estimated for the design of microwave filters in the frequency domain. Finally, time-domain design was applied to microwave filters in [12], but using commensurate line lengths; in other words, the length of the transmission line is not a variable, which can generate a narrowband design.

In section 2 of this paper, the time-domain technique is explained and in section 3, the capability of this method is illustrated by a microstrip-line filter design using this technique. Comparisons are made based on the simulation results attained using Agilent ADS software. Finally, the paper concludes with section 4.

2. TIME-DOMAIN DESIGN TECHNIQUE

How to design an UWB filter given the frequency-domain response? The characteristics of a filter can easily be specified in the frequency domain. One can use conventional frequency-domain techniques to design filters mainly as different connections, series or parallel, of RLC elements [5, 6]. If the required bandwidth is very large compared to the center frequency, this design technique becomes difficult to apply. On the other hand, very large bandwidth means narrow time-domain signals, and opens up the opportunity of a time-domain design technique. The first step in such a time-domain design technique is to obtain the time-domain response from a given frequency spectrum. Specifically, if a short-pulse UWB system is concerned, the frequency spectrum of the filter can be easily specified as the reflection coefficient S_{11} of the filter in the frequency domain. Assuming an incident voltage
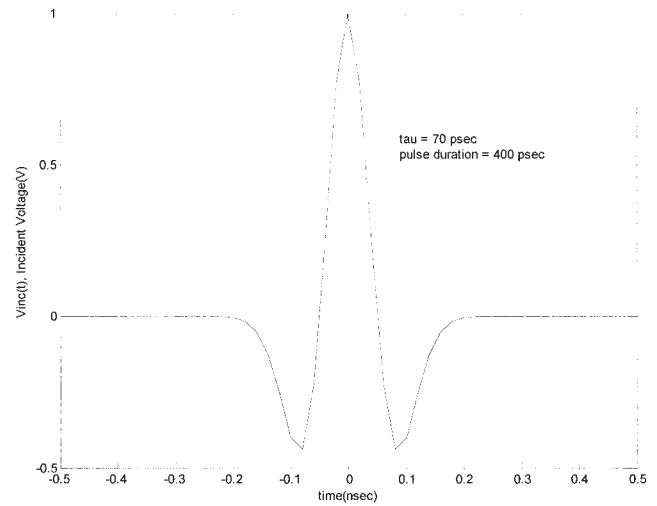
Figure 1 Incident UWB Gaussian monopulse waveform with $\tau = 70$ psec

$v_{inc}(t)$ of an UWB Gaussian pulse (which is a commonly used pulse type for UWB systems), the reflected voltage $v_{ref}(t)$ can be easily found in the time domain. Figure 1 shows the time domain waveform of such an UWB monopulse for duration of 400 picosec. This UWB monopulse waveform, $v_{inc}(t)$, is obtained as the second derivative of a Gaussian waveform, given by

$$V(t) = e^{-(t/\tau)^2} \text{ Volts,} \qquad (1)$$

and its second derivative is given as

$$v_{inc}(t) = V''(t) = \frac{d}{dt}\left[\frac{t}{\tau} e^{-(t/\tau)^2}\right] \text{ Volts,} \qquad (2)$$

where τ is the parameter proportional to the time duration of the Gaussian pulse and is 70 psec in Figure 1. The reflected voltage frequency spectrum, $b_1(f)$, is simply obtained from reflection coefficient by

$$b_1(f) = S_{11}(f)a_1(f), \qquad (3)$$

where $a_1(f)$ is the incident voltage in the frequency domain, and the $S_{11}(f)$ is the reflection coefficient in the frequency domain. Figure 2 shows the frequency spectra of the incident and reflected voltages and the reflection coefficient $S_{11}(f)$. Figure 2(a) shows the frequency spectrum of the incident voltage, which is the second derivative of the Gaussian pulse. The reflection coefficient $S_{11}(f)$ is shown in Figure 2(b), and the frequency spectrum of reflected voltage is illustrated in Figure 2(c). Also shown in Figure 2(d) is the frequency spectrum of transmitted voltage into the circuit, which is calculated as follows:

$$c_1(f) = \sqrt{a_1^2(f) - b_1^2(f)}. \qquad (4)$$

By employing inverse Fourier transform, the reflected voltage waveform in the frequency domain can be easily converted into a time-domain signal. The reflected voltage, shown in Figure 3(a), is actually the multiple reflections of the incident-voltage time waveform from multiple discontinuity points in a circuit (which means different time delays) with different coefficients. These discontinuity points and corresponding reflection coefficients can be iden-
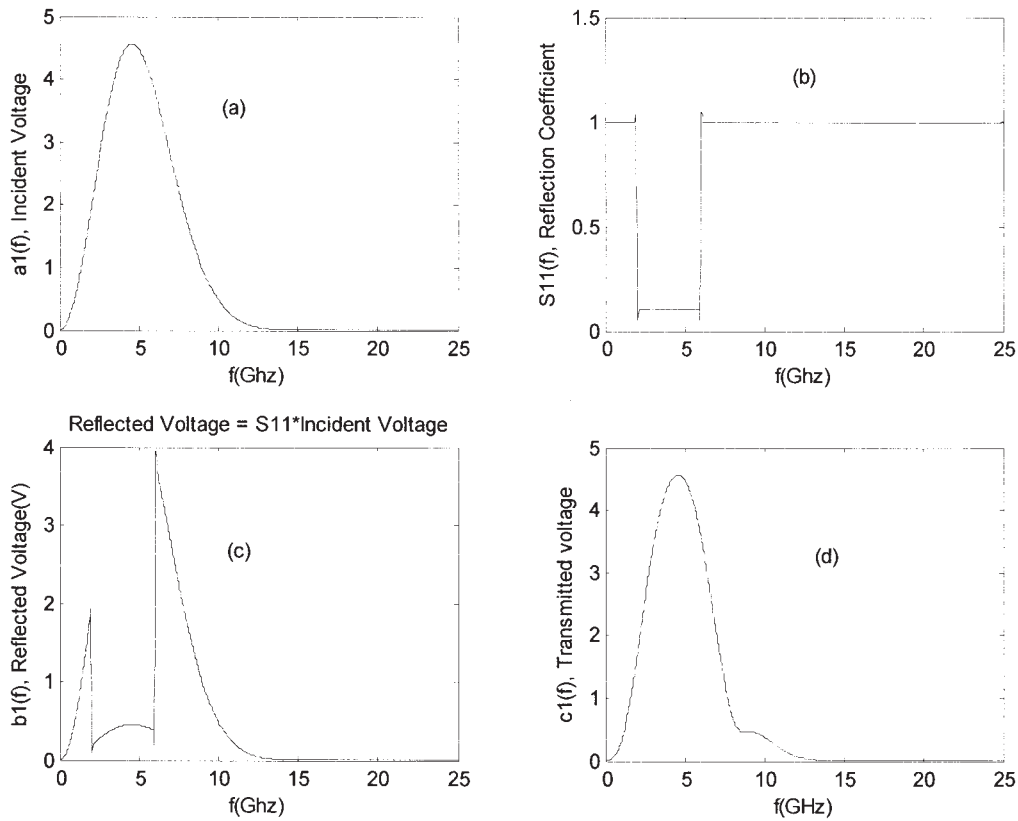
Figure 2 Frequency spectra of (a) incident voltage; (b) reflection coefficient; (c) reflected voltage; (d) transmitted voltage

tified from the reflected voltage waveform by taking the correlation of the reflected voltage with the incident voltage. This can be clearly seen in Figure 3(b), where a scaled incident voltage (peak amplitude = 1) and the reflected voltage (peak amplitude = 0.5) are plotted in the same figure for comparison. It is seen that the first strong correlation is at time = 20.5 nsec, with a peak correlation of 0.5. Now, the next step is to subtract this first strong correlation from the total reflected voltage waveform to find the rest of the discontinuity points. Figure 3(c) shows the plot of the total reflected voltage waveform, excluding the first discontinuity point.
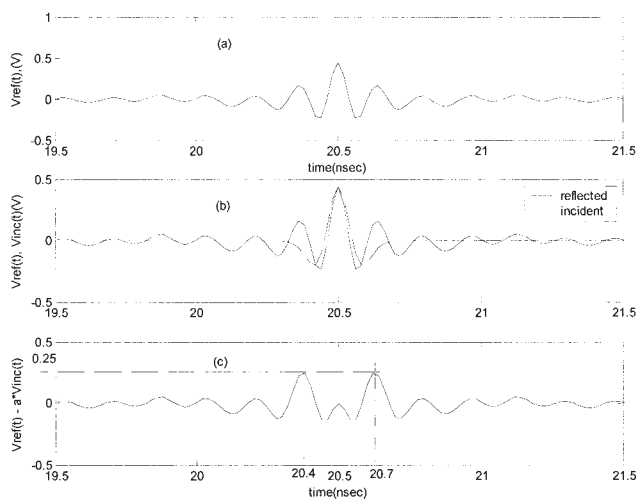
Figure 3 Time-domain waveforms of (a) a typical reflected voltage; (b) reflected and incident voltages; (c) reflected voltage minus a scaled incident voltage at 20.5 nsec

In this figure, there are two discontinuity points at 20.7 and 20.4 nsec with peak amplitudes of 0.25. For the sake of simplicity, only the 1st-order reflections will be taken into consideration, and the correlation of this reflected voltage waveform will create two more discontinuity points (corresponding time delays) with different reflection coefficients. This procedure can be repeated until an error criterion is satisfied. The error criteria can be such that the reflected voltage waveform is expressed as a sum of multiple different delayed versions of the incident waveform with different amplitudes, and the error between the reflected voltage and its approximation as a sum of a finite number of delayed incident voltages with different amplitudes will be small.

After obtaining the reflected voltage waveform as a sum of delayed versions of incident voltage with different amplitudes, these can be interpreted as the sections of the microstrip line filters, that is, the number of UWB pulses that are present in the reflected voltage waveform will give the number of sections of the transmission line, the different amplitudes will give the reflection coefficients of these transmission line sections, and the time delays will be the length of the transmission-line sections. Conversion of the reflection coefficient amplitudes and time delays into transmission-line parameters can be performed using transmission-line models by using 1st-order reflections only. The reflection coefficient between the two transmission lines with different characteristic impedances is given by

$$\Gamma_{12} = \frac{Z_2 - Z_1}{Z_2 + Z_1}, \tag{5}$$

where Z_1, Z_2 are the characteristic impedances of the transmission lines. The transmission coefficient from the first transmission line

into the second transmission line is given in terms of the reflection coefficient by

$$T_{12} = 1 + \Gamma_{12}. \qquad (6)$$

As an example, we can use three transmission lines to model the reflections. Since only 1st-order reflections are considered, the first reflection will be from the discontinuity between the first two transmission lines and its amplitude will be given by

$$R_1 = \Gamma_{12}. \qquad (7)$$

The second reflection will come from the junction between the second and third transmission lines and its amplitude, R_2, is equal to

$$R_2 = T_{12}\Gamma_{23}(1 - \Gamma_{12}) = (1 + \Gamma_{12})\Gamma_{23}(1 - \Gamma_{12})$$
$$= (1 - \Gamma_{12}^2)\Gamma_{23}, \qquad (8)$$

where Γ_{23} is the reflection coefficient between the second and third transmission lines. Eq. (7) gives us the solution for Γ_{12} and Eq. (8) can be rewritten to yield the solutions for Γ_{23} as follows:

$$\Gamma_{23} = R_2/(1 - R_1^2). \qquad (9)$$

Once the solutions are obtained for Γ_{12}, Γ_{23}, the characteristic impedances of the second and third transmission lines can be easily found using

$$Z_2/Z_1 = \frac{1 + \Gamma_{12}}{1 - \Gamma_{12}},$$

$$Z_3/Z_2 = \frac{1 + \Gamma_{23}}{1 - \Gamma_{23}}. \qquad (10)$$

For the final part of the design, the length of the transmission lines should also be specified. This is obtained from the time delays Δt of the UWB pulses with respect to each other. The earliest reflection comes from junction of first and second transmission lines, the second earliest reflection comes from the second and third transmission line sections, and so forth. Hence, these time delays are
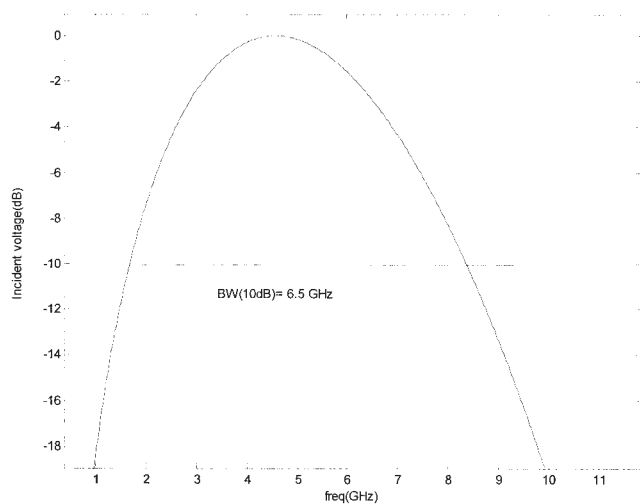
Figure 4 Incident UWB pulse waveform with center frequency of 4.6 GHz and a bandwidth of 6.5 GHz

TABLE 1 Transmission-Line Impedances and Lengths

	Δt_i [psec]	R_i [reflections]	Γ_{ij}	Z_i [Ohms]	Δl_i [cm]
$i = 1$	0	0.248	$\Gamma_{12} = 0.248$	82.9758	0
$i = 2$	120	0.4439	$\Gamma_{23} = 0.473$	139.7579	0.84
$i = 3$	240	0.248	$\Gamma_{34} = 0.3405$	101.619	1.68

functions of the transmission-line lengths. The time delays are converted into lengths of the transmission lines using

$$\Delta l = (\Delta t/2)\frac{c}{\sqrt{\varepsilon_r}}, \qquad (11)$$

where Δt is the round trip time from the junction of the transmission lines, c is the speed of the light, and ε_r is the relative dielectric constant of the substrate. In the next section, the design technique will be illustrated by an example.

3. VERIFYING THE DESIGN TECHNIQUE

The time-domain technique is applied to design an UWB microstrip band pass filter from 2 to 6 GHz. The desired characteristics is such that $S_{11} < (1/10)$ (-10 dB) between 2 and 6 GHz and, outside of the pass band, $S_{11} = 1$ (0 dB). For the implementation of the filter, a dielectric of $\varepsilon_r = 4.6$ and thickness of 1.55-mm FR4 substrate are used for the impedance and length of the transmission-line calculations. The filter is assumed to be excited with an UWB pulse and the frequency spectrum of the UWB pulse is shown in Figure 4. The 10-dB bandwidth is around 6.5 GHz with a center frequency of 4.6 GHz. By applying the procedure outlined in section 2, the time delays Δt between the UWB pulses, the reflection coefficients R_i, and the corresponding Γ_{ij} and Z_i for $i = 1, 2, 3$ calculated using Eqs. (7–10) are shown in Table 1. Also using these impedance values and the lengths, the transmission-line circuit is simulated in ADS, as shown in Figure 5. In the circuit, there are two transmission-line sections, with impedances $Z_1 = 82.9758\Omega$ and $Z_2 = 139.7579\Omega$ and a terminating impedance $Z_3 = 101.619\Omega$, with section lengths of 0.84 and 1.68 cm, which are calculated using Eq. (10).

Three discontinuity points are specified for an error of peak amplitude 0.015. Initially, the reflected voltage waveform has a peak of 0.5 (with only one UWB pulse approximation), the maximum error dropped to 0.2, and the three-term error was approximately 0.015. Increasing number of terms will decrease the error; however, it will also increase the number of coefficients and hence the transmission-line sections. Now, the question is how good are these error criteria; in other words, how good is this three-point reflection approximation with the desired S_{11} specifications and also how good is the filter designed using this technique. Figure 6 illustrates the answer to this question. First, the desired filter response is plotted with the solid line, the other two curves plots the S_{11} calculated from three discontinuity points only (dashed
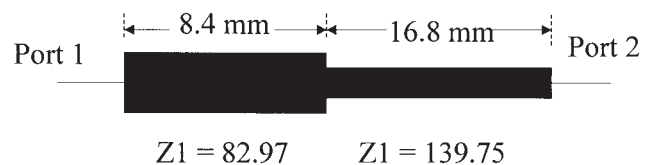

Figure 5 UWB microstrip filter simulated in Agilent ADS as two transmission-line sections on a grounded dielectric of $\varepsilon_r = 4.6$ and thickness of 1.55 mm
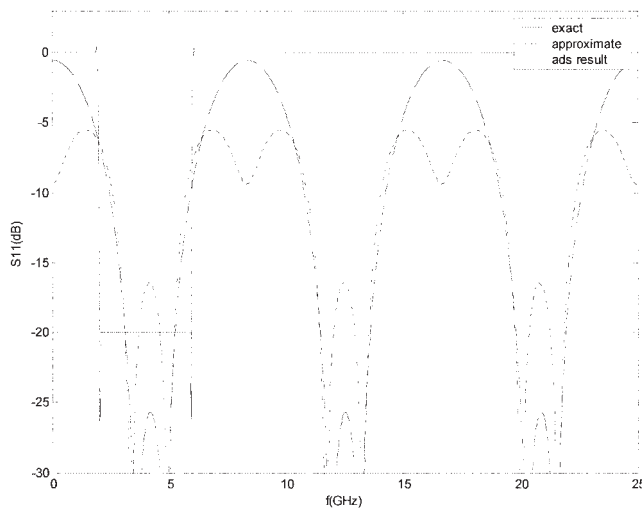
Figure 6 The magnitude of S_{11} vs. frequency: desired response (solid line), UWB pulse approximation method (dashed line), ADS simulations (dotted line)

line), and the S_{11} calculated from the transmission line filter implemented in Agilent ADS (dotted line). As can be seen from the figure, the S_{11} values from the reflections and the ADS simulations are very close, and are also below 10 dB in the passband frequencies of 2.5 to 5.75 GHz. The small difference between them are the results of the fact that the three-point reflection S_{11} has only 1st-order reflections only; on the other hand, in the ADS simulations, there are infinitely many orders of reflection in the circuit.

It is seen that it is possible design a UWB filter using only three terms with a return loss of greater than 10 dB. For further accuracy, the number of reflections for approximation can be increased. The phase of S_{11} is also plotted in Figure 7, where the solid line is the phase of S_{11} from the ADS implemented circuit, and the dashed line is the phase of S_{11} calculated from the three-point reflections. Reflection coefficient S_{11} has a linear phase over the passband frequencies for ADS simulations, whereas the approximate reflections have a large phase error over the passband frequencies. However, the phase error is minimized in an average sense for reflection approximation, as can be seen from the figure.
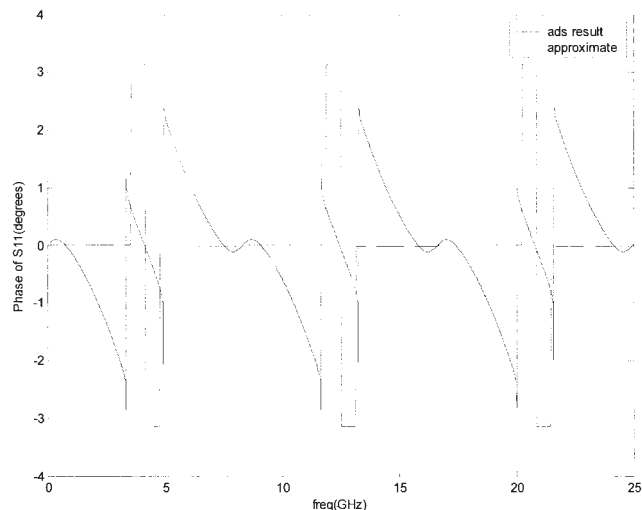
Figure 7 Phase of S_{11} calculated from ADS simulations (solid line) and UWB pulse approximation method (dashed line)

Initially, the design procedure is based on the amplitude only and the initial phase for all frequencies is taken as zero. A better choice of the phase of S_{11} may improve the approximation accuracy. Finally, the assumption that the phase velocity in the microstrip line is $c/\sqrt{\varepsilon_r}$ will also contribute to the errors in addition to a few term approximations for the reflections.

4. CONCLUSION

We have proposed a novel time-domain technique which can be used to design UWB microstrip filters. The technique is based on obtaining the time-domain reflected voltage waveform of a circuit, given the reflection coefficient and assumed incident waveform of a Gaussian pulse in the frequency domain. By resolving multiple discontinuity points with different amplitudes and time delays, the total reflected waveform can be represented as a sum of these discrete reflections from the circuits. This technique has been applied to the design of an UWB microstrip filter between 2 and 6 GHz as an example, and S_{11} of 10 dB or better has been obtained over the passband with only three reflection points. Also, reasonable agreement has been obtained between the S_{11} result obtained from the reflection approximations and the S_{11} result from the microstrip-line filter simulated in ADS.

REFERENCES

1. H.L. Bertoni, L. Carin, and L.B. Felsen (Editors), Ultra-wideband short pulse electromagnetics, Kluwer Publications, New York, 1992.
2. C.L. Bennett and G.F. Ross, Time-domain electromagnetics and its applications, Proc IEEE 66 (1978), 29–318.
3. Ultra wideband tutorial, IEEE P802.15 Working group for WPAN document, doc. no. IEEE 802.15-00/083r0, 2000.
4. J. Foerster et al., Ultra-wideband technology for short- or medium-range wireless communications, Intel Technology J Q2 (2001).
5. D.M. Pozar, Microwave engineering, 2nd ed., Wiley, New York, 1998.
6. R. Levy, R.V. Snyder, and G. Matthaei, Design of microwave filters, IEEE Trans Microwave Theory Tech 50 (2002), 783–793.
7. T.A. Cusick, S. Iezekiel, and R.E. Miles, All-optical microwave filter design employing a genetic algorithm, IEEE Photon Technol Lett 10 (1998), 1156–1158.
8. S. Chahravarty and R. Mittra, Design of microwave filters using a binary coded genetic algorithm, IEEE Antennas Propagat Soc Int Symp Dig 1 (2000), 144–147.
9. M.E. Mokari and M. Rubin, Design and realization of transversal microwave bandpass filters, IEEE Int Symp Circ Syst 2 (1990), 1513–1516.
10. R. Tascone, P. Savi, D. Trinchero, and R. Orta, Scattering matrix approach for the design of microwave filters, IEEE Trans Microwave Theory Tech 48 (2000), 423–430.
11. P.P. Roberts and G.E. Town, Design of microwave filters by inverse scattering, IEEE Trans Microwave Theory Tech 43 (1995), 739–743.
12. N.I. Sobhy and E.A. Hosny, Microwave filter design in the time domain, IEEE MTT-S Int Microwave Symp Dig 81 (1981), 57–59.